EPJ Web of Conferences **35**, 05005 (2012)
DOI: 10.1051/epjconf/20123505005

Sub-barrier transfer in ^{16}O+^{208}Pb and ^{32}S+^{208}Pb and its role in understanding the suppression of fusion

M. Evers[1,a], M. Dasgupta[1], D. J. Hinde[1], and C. Simenel[1,2]

[1] Department of Nuclear Physics, Research School of Physics and Engineering, The Australian National University, Canberra, ACT 0200, Australia
[2] CEA, Centre de Saclay, IRFU/Service de Physique Nucleaire F-91191 Gif-sur-Yvette, France

Abstract. A detailed analysis of the projectile-like fragments detected at backward angles in the reactions ^{16}O,^{32}S+^{208}Pb at energies below the fusion barrier is presented. Excitation functions corresponding to nucleon transfer with $\Delta Z = 1$ and $\Delta Z = 2$ were extracted, indicating surprisingly large absolute probabilities at sub-barrier energies. A comparison of $2p$ transfer probabilities with time-dependent Hartree-Fock calculations suggests strong pairing correlations between the two protons. Excitation energies in the projectile-like fragments up to $\sim$ 15 MeV for the ^{16}O and $\sim$ 25 MeV for ^{32}S-induced reactions demonstrate the population of highly excited states in the residual nuclei, indicating substantial dissipation of kinetic energy. These highly inelastic (large excitation energies) and complex (correlated few-nucleon transfer) processes may be closely related to the depletion of fusion through tunnelling at sub-barrier energies.

1 Introduction

Heavy-ion collisions provide an interesting field to study the effects of quantum-mechanical properties as well as classical phenomena, and how they emerge in the dynamics of the collision process at different energies. At energies *well below and close to* the fusion barrier, heavy-ion collisions are entirely driven by quantum mechanics. For example, fusion at sub-barrier energies occurs through tunnelling through the fusion barrier. Furthermore, sub-barrier fusion as well as its complementary process, scattering, are affected by the internal structure of the collision partners [1,2]. In describing sub- and near-barrier nuclear collisions, the coupled reaction channels formalism, where colliding nuclei are considered to be in a coherent superposition of their intrinsic states, has proven extremely successful. However, at deep sub-barrier energies (e.g. $\sim$ 5 MeV below the fusion barrier energy in the reaction ^{16}O+^{208}Pb) measured fusion cross sections [3–6] fall below those predicted by coupled reaction channels calculations using standard Woods-Saxon potentials. This deep sub-barrier fusion suppression has been observed in a range of different reactions. A major question in nuclear physics is to explain the physical mechanisms causing this suppression of fusion, since extrapolations of fusion probabilities to energies typical for astrophysical scenarios show large variations (up to 40 orders of magnitude) between different phenomenological models [7–9].

At energies *above* the fusion barrier fusion cross sections are also significantly below standard coupled-channels calculations [5,10] using the same Woods-Saxon parametrization for the nuclear potential. A detailed analysis of this above-barrier fusion suppression for different reactions shows an increase of the suppression factor with the charge product of the colliding nuclei. Correlated with increasing above-barrier fusion suppression is increasing dissipation of kinetic energy into nucleonic degrees of freedom, known as deep inelastic collisions (DIC) [10,11]. This becomes important with increasing matter overlap at energies near and above the fusion barrier energy. The importance of (multi-) nucleon transfer in these DIC processes at energies well above the fusion barrier has been discussed in a recent review [12]. Transfer processes that lead to high excitation energies in the residual nuclei were suggested [10,13] as a key to understanding the above-barrier fusion suppression through the onset of irreversible dissipative processes.

In this paper recent results are discussed which suggest that mechanisms used to explain above-barrier fusion suppression may also be responsible for the suppression of fusion through tunnelling at deep sub-barrier energies. Using the reactions ^{16}O,^{32}S+^{208}Pb, (i) the significance of transfer processes in nuclear collisions at energies well below the fusion barrier is established, and (ii) the details and underlying mechanisms of these transfer processes are explored.

2 Measurements

All measurements were done at the 14UD electrostatic accelerator of the Heavy-Ion Accelerator Facility at the Australian National University (ANU), using beams of ^{16}O and ^{32}S incident on a ^{208}PbS target with a thickness of 100 μg/cm^2, evaporated onto a 15 μg/cm^2 C backing. A $\Delta E - E$ detector telescope consisting of a propane gas filled ionization chamber and a Si detector located at a backward angle of $\theta_{\rm lab} = 162^\circ$ was used to record the energy $E_{\rm Si}$ and energy loss $\Delta E_{\rm gas}$ of the back-scattered projectile-like fragments (PLFs). Two Si monitors positioned at $\pm 30^\circ$ were used to normalize the back-scattered events to the Rutherford cross section. A typical two dimensional spectrum for a measurement of the reaction ^{16}O+^{208}Pb at a beam energy corresponding to a ratio of the centre-of-mass energy to the fusion barrier energy $E_{c.m.}/V_B = 0.98$ is shown in Fig. 1. The three distinct regions correspond to oxygen, nitrogen and carbon PLFs, which are associated with the transfer of $\Delta Z = 0$, 1 and 2 units of charge. The peak at $E_{\rm Si} \sim 50$ MeV is due to elastically scattered ^{16}O particles, the smaller peak at $E_{\rm Si} \sim 48$ MeV is associated with the excitation of the lowest 3^- excited state in ^{208}Pb at an

[a] e-mail: maurits.evers@anu.edu.au

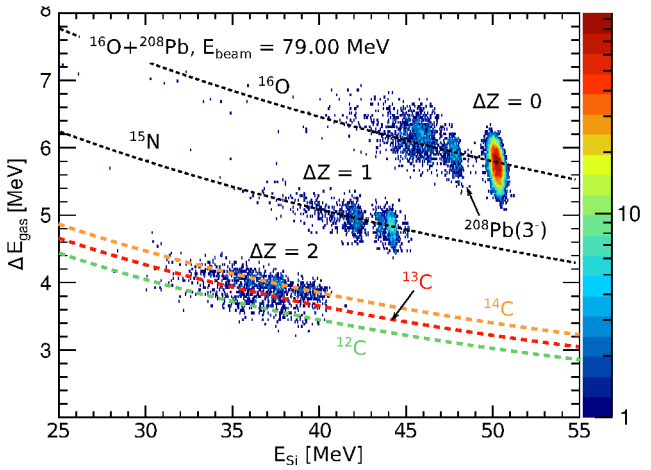

Fig. 1. Typical $\Delta E - E$ spectrum for the reaction ^{16}O+^{208}Pb at the indicated beam energy, corresponding to $E_{c.m.}/V_B = 0.98$. Events corresponding to the transfer of $\Delta Z = 0$, 1 and 2 units of charge are labelled. Calculated energy loss curves for ^{16}O, ^{15}N and ^{12,13,14}C are shown by the dashed curves.

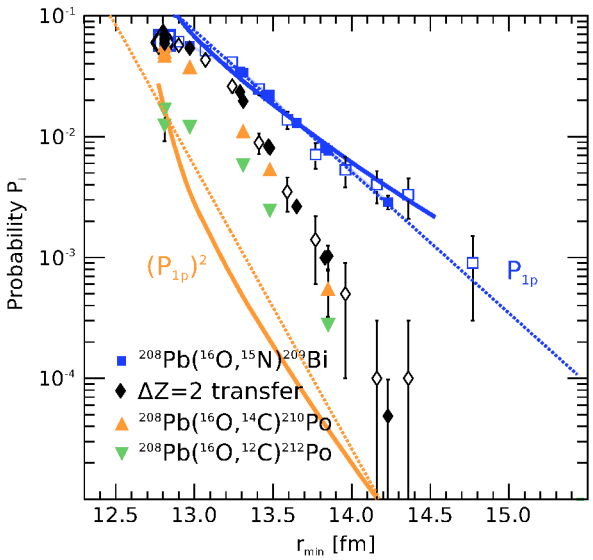

Fig. 2. Transfer probabilities P_i for the indicated transfer processes in the reaction ^{16}O+^{208}Pb as a function of the distance of closest approach (see text). The asymptotic behaviour for $1p$ transfer and predicted sequential $2p$ transfer are shown by the dotted straight lines. TDHF calculations for $1p$ and $2p$ transfer are shown by the solid blue and orange curves. The large open square and diamond symbols at $r_{min} = 12.8$ fm are the measurements for N (blue) and C PLFs (black) from Videbaek et al. [15]. The smaller open squares and diamonds are the measurements for N (blue) and C PLFs (black) from Timmers [16].

excitation energy of 2.615 MeV. Events resulting from the transfer of three or more charged nucleons ($\Delta Z \geq 3$) are not observed for measurements at sub-barrier energy. Spectra for measurements of the PLFs following the reaction ^{32}S+^{208}Pb show similar features.

3 Transfer probabilities

3.1 Z identification of the PLFs

Transfer probabilities for processes with different ΔZ were extracted by gating on the particular region of interest in the $\Delta E - E$ spectra, and normalizing the number of events to the total number of counts in the two forward angle monitor detectors. Overall normalization of the probabilities was obtained from measurements of the total quasi-elastic scattering yields at energies well below the barrier energy, following the procedure detailed in Ref. [14]. For the reaction ^{16}O+^{208}Pb, deduced transfer probabilities for $\Delta Z = 1$ (nitrogen PLFs) and $\Delta Z = 2$ (carbon PLFs) are shown in Fig. 2, plotted as a function of the distance of closest approach $r_{\rm min}$ assuming a trajectory in a Coulomb plus nuclear potential. A Woods-Saxon parametrization of the nuclear potential was used

$$V_N(r) = -\frac{V_0}{1+\exp\frac{r-R_0}{a_0}}, \qquad (1)$$

where the parameters V_0, r_0 and a_0 were determined from analyses of the total quasi-elastic (and in the case of the reaction ^{16}O+^{208}Pb the inelastic ^{208}Pb(3$^-$)) scattering excitation functions within a coupled-channels framework as described in Refs. [2,14,17]. At energies well below the fusion barrier, $r_{\rm min}$ approaches the minimum distance assuming a pure Coulomb trajectory

$$r_{\rm min} \xrightarrow[E_{c.m.} \ll V_B]{} r_{\rm min}^{\rm Coul} = \frac{Z_p Z_t e^2}{4\pi\epsilon_0}\frac{1}{2E_{c.m.}}\left(1+\mathrm{cosec}\,\frac{\theta_{c.m.}}{2}\right),$$

where Z_p, Z_t are the atomic numbers of projectile and target nucleus, and $E_{c.m.}$ and $\theta_{c.m.}$ are the energy and scattering angle in the centre-of-mass frame, respectively. As the energy increases $r_{\rm min}$ becomes smaller than $r_{\rm min}^{\rm Coul}$ due to the attractive nuclear potential. The obtained absolute probabilities show excellent agreement with measurements from Refs. [15,16].

3.2 Absolute transfer probabilities for transfer processes in the reaction ^{16}O+^{208}Pb

Reaction Q-values for $\Delta Z = 1$ transfer processes in the reaction ^{16}O+^{208}Pb are well separated, allowing the identification of the predominant contribution to the $\Delta Z = 1$ events with the transfer of one proton ($1p$-stripping). For $\Delta Z = 2$, discrete peaks are not prominent in the excitation energy spectra (see top panel of Fig. 3), but an isotopic separation of the different carbon PLFs was possible using the calculated energy loss curves for different carbon isotopes as shown in Fig. 1. The contributions from ^{12}C, ^{13}C and ^{14}C to the integrated $\Delta Z = 2$ counts were determined as discussed in Ref. [18,19]. Extracted transfer probabilities for the two dominant processes, $2p$-stripping ^{208}Pb(^{16}O,^{14}C)^{210}Bi, and α-particle stripping ^{208}Pb(^{16}O,^{12}C)^{212}Bi are shown in Fig. 2 by the orange and green triangles, respectively. Transfer probabilities for the $2p1n$-stripping process ^{208}Pb(^{16}O,^{13}C)^{211}Bi are $\sim$ 10 times smaller than those for α-particle transfer and are not shown. Contrary to what was commonly assumed [20–23] at sub-barrier energies, $2p$ transfer is the dominant process, α-particle transfer probabilities being smaller by a factor of $\sim 2-3$. The difference in probabilities between $2p$ and α transfer increases with increasing beam energy, and is largest at $E_{c.m.}/V_B \sim 1.0$.

3.3 Absolute transfer probabilities for transfer processes in the reaction ^{32}S+^{208}Pb

For the reaction ^{32}S+^{208}Pb, an equivalent analysis also indicates that $2p$-stripping is the dominant $\Delta Z = 2$ transfer

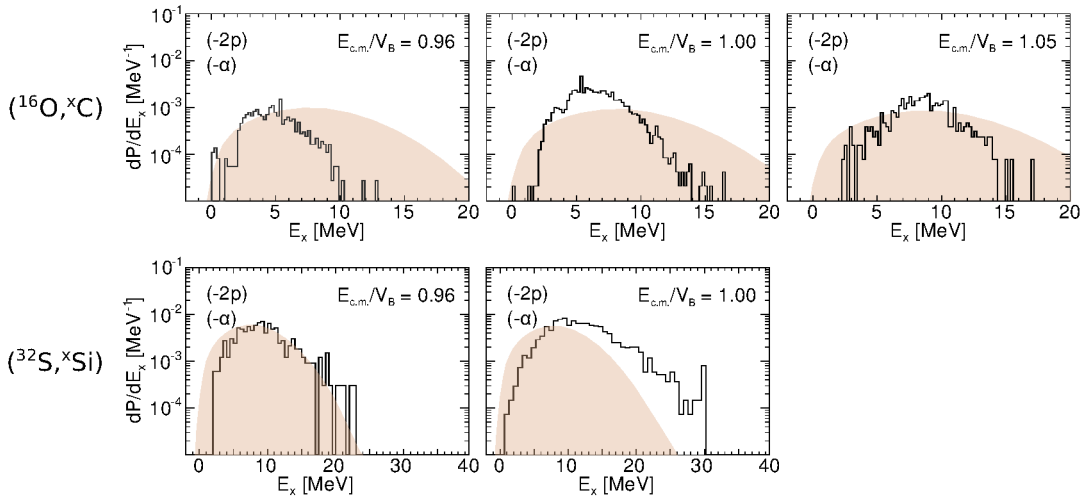

Fig. 3. Excitation energy spectra showing the differential transfer probabilities dP/dE_x as a function of the excitation energy E_x (i.e. kinetic energy loss taking into account the specific reaction Q value) of the PLFs for the indicated energies with respect to the fusion barrier energy $E_{c.m.}/V_B$ for the $\Delta Z = 2$ transfer processes ($2p$, α transfer) in the reactions ^{16}O+^{208}Pb (top panel) and ^{32}S+^{208}Pb (bottom panel). The shaded areas show results from GRAZING calculations, see text for details.

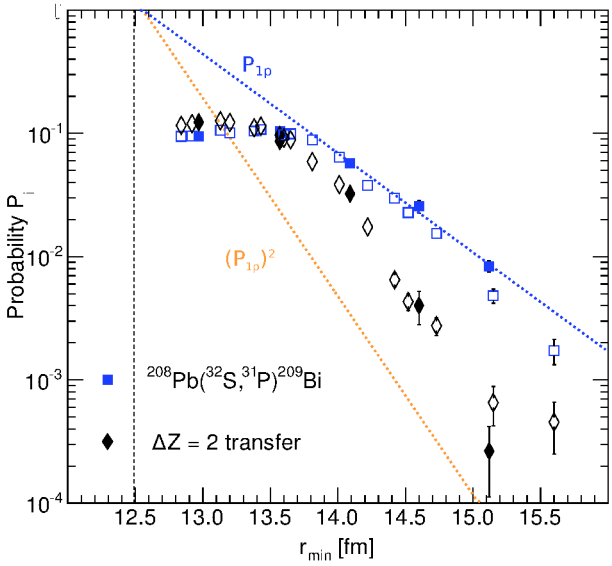

Fig. 4. Transfer probabilities P_i for the indicated transfer processes in the reaction ^{32}S+^{208}Pb as a function of the distance of closest approach $r_{\rm min}$ (see text). The asymptotic behaviour for $1p$ transfer and predicted sequential $2p$ transfer are shown by the dotted straight lines. The open square and diamond symbols are the measurements for P and Si PLFs from Timmers [16].

process compared to α-particle transfer. In neither the $\Delta Z = 1$ nor the $\Delta Z = 2$ events discrete peaks could be seen in the excitation energy spectra (as can be seen in the bottom panel of Fig. 3 for $\Delta Z = 2$ transfer in ^{32}S+^{208}Pb). Due to the similarity in reaction Q-values of different transfer processes for both $\Delta Z = 1$ and $\Delta Z = 2$, deduced transfer probabilities may contain contributions from the channels $-1p$ and $-1p + 1n$ for $\Delta Z = 1$ and $-2p - 1n$ and $-2p + 2n$ for $\Delta Z = 2$, respectively. Resulting extracted transfer probabilities for $\Delta Z = 1$ and $\Delta Z = 2$ transfer are shown in Fig. 4.

3.4 Time-dependent Hartree-Fock calculations

TDHF calculations were performed for the reaction ^{16}O+^{208}Pb which allow the calculation of transfer excitation functions for $1p$ and $2p$ transfer using particle number projection techniques on the PLFs [24]. Since TDHF calculations are based on an independent particle picture, calculated $2p$ transfer probabilities comprise sequential transfer of two uncorrelated protons.

Results for the $1p$ and $2p$ transfer probabilities are shown by the solid blue and orange curves in Fig. 2. As detailed in Ref. [19] all TDHF results were scaled by a factor of 0.43 to match the experimental $1p$ transfer probabilities in the interval $13.2 < r_{\rm min} < 14.2$ in which absorptive processes are negligible. The energy dependence of the TDHF calculations agree with the $1p$ transfer probabilities. The measured $2p$ probabilities are much higher than the TDHF calculations, indicating that in reality there is a strong pairing correlation between the two transferred protons, which leads to the enhanced $2p$ transfer probabilities. The TDHF calculations for $2p$ transfer are in close agreement with the predicted sequential $2p$ transfer probabilities $(P_{1p})^2$ (shown by the dotted orange line in Fig. 2), where P_{1p} is the experimentally measured $1p$ transfer probability.

Overall, the agreement between TDHF calculations and the energy dependence of the extracted transfer probabilities for $1p$ transfer at energies below the fusion barrier is good. The calculated $2p$ transfer probabilities underpredict the extracted $2p$ transfer probabilities and therefore independently confirm a strong pairing correlation of the two protons in the observed $2p$ transfer probabilities.

4 Excitation energies

The energies lost to excitation of the residual nuclei following $\Delta Z = 1$ and $\Delta Z = 2$ transfer were determined using transfer leaving the residual nuclei in their ground states as the reference. Where populated, the ground-state transfers provided a good check of the energy calibration. From the excitation energy spectra, the differential transfer probabilities dP/dE_x were determined. Fig. 3 shows excitation energy spectra dP/dE_x as a function of E_x for energies corresponding to $E_{c.m.}/V_B = 0.96, 1.00, 1.05$ for the PLFs following $\Delta Z = 2$ transfer in the ^{16}O- (top panel) and ^{32}S-induced reactions (bottom panel).

As can be seen from Fig. 3, average excitation energies increase with increasing charge product of the colliding nuclei, associated with increasing matter overlap between target and projectile nucleus. All reactions show the

population of highly excited states, even at beam energies well below the fusion barrier. At an energy $\sim$ 5 MeV below the barrier, excitation energies up to $\sim$ 15 MeV are observed for the ^{16}O-induced reaction and $\sim$ 25 MeV for the ^{32}S-induced reaction.

Simple optimum Q-value considerations as detailed in Ref. [19] show that there is a significant contribution to the total differential transfer probabilities dP/dE_x from processes leading to excitation energies *higher* than the optimum Q-value based excitation energy.

4.1 GRAZING calculations

Calculations were performed using the code GRAZING [25, 26], which is based on a semi-classical model. The code allows to include couplings to both single-nucleon transfer channels and collective excited states of the interacting nuclei. Multi-nucleon transfer occurs via a multi-step process, i.e. calculated $2p$ transfer probabilities imply sequential transfer of two uncorrelated protons. The resulting coupled equations are solved in the semi-classical approximations for the relative motion of the interacting nuclei. It is important to note that GRAZING calculations give differential transfer cross sections as a function of excitation energy of the PLFs integrated over all impact parameters (i.e. angular momenta). A comparison with the measured excitation energy spectra at the angle of $\theta_{\rm lab} = 160.6^\circ$ is justified since the $2p$ transfer angular distributions are strongly peaked at backward angles at the measured energies, see Ref. [15].

GRAZING calculations following $\Delta Z = 2$ transfer in the reactions ^{16}O,^{32}S are shown in Fig. 3. All GRAZING differential transfer cross sections were scaled by the same factor, which was determined such that GRAZING calculations reproduce the total measured $2p$ transfer probability in the reaction ^{32}S+^{208}Pb at $E_{c.m.}/V_B = 0.96$. GRAZING differential transfer cross sections were folded with a Gaussian distribution to account for the experimental energy resolution of 1 MeV. Overall, GRAZING calculations fail to correctly reproduce the observed trend of increasing average excitation energy with increasing charge product of the projectile and target nuclei. Moreover, and similar to the previous optimum Q-value considerations, at large excitation energies calculated differential transfer probabilities fall below those extracted from the measured excitation energy spectra for the reaction ^{32}S+^{208}Pb. This is consistent with GRAZING results for the kinetic energy loss spectra of the PLFs following $2p$ transfer in the reaction ^{40}Ca+^{208}Pb in Ref. [27], which also show large discrepancies at high excitation energies between the calculated and measured differential transfer cross sections as a function of excitation energy for measurements at beam energies near the fusion barrier.

The failure to properly reproduce the measured large kinetic energy losses in the PLFs following $2p$ transfer (corresponding to large excitation energies in the residual nuclei) indicates dissipative processes in $2p$ transfer which are not included in the GRAZING model.

5 Conclusion

In conclusion, the following results were obtained from a detailed analysis of the projectile-like fragments detected at a backward angle in the reactions ^{16}O,^{32}S+^{208}Pb:

1. Transfer of two protons ($2p$-stripping) in the reactions ^{16}O,^{32}S+^{208}Pb occurs with a significant probability already at energies well below the fusion barrier. $2p$ transfer is the predominant $\Delta Z = 2$ transfer process, with absolute probabilities being $\sim 2-3$ times larger than those for α-particle transfer.
2. The transfer excitation functions for $2p$ transfer in ^{16}O+^{208}Pb suggest a strong pairing correlation of the two transferred protons. This is supported by TDHF calculations based on the independent particle picture.
3. The residual nuclei following $2p$ and α-particle transfer are left in highly excited states, with excitation energies up to $\sim$ 15 MeV and $\sim$ 25 MeV for the ^{16}O- and ^{32}S-induced PLFs, respectively. A comparison with $Q_{\rm opt}$ and GRAZING calculations show projectile-like fragments with larger kinetic energy losses than expected based on these semi-classical considerations. This suggests that dissipative and irreversible processes play an important role already at energies well below the fusion barrier.

These considerations strongly support the idea that few-nucleon transfer triggers the onset of dissipative and irreversible processes in the collision of nuclei already at energies well-below the fusion barrier. This would reduce the tunnelling probability, and suppress the fusion yield at these energies.

References

1. M. Dasgupta *et al.*, Annu. Rev. Nucl. Part. Sci. **48**, 401 (1998).
2. M. Evers *et al.*, Phys. Rev. C **78**, 034614 (2008).
3. C. L. Jiang *et al.*, Phys. Rev. Lett. **89**, 052701 (2002).
4. C. L. Jiang *et al.*, Phys. Rev. C **71**, 044613 (2005).
5. M. Dasgupta *et al.*, Phys. Rev. Lett. **99**, 192701 (2007).
6. H. Esbensen *et al.*, Phys. Rev. C **76**, 054609 (2007).
7. C. L. Jiang *et al.*, Phys. Rev. C **75**, 015803 (2007).
8. C. L. Jiang *et al.*, Phys. Rev. C **79**, 044601 (2009).
9. L. R. Gasques *et al.*, Phys. Rev. C **76**, 035802 (2007).
10. J. O. Newton *et al.*, Phys. Rev. C **70**, 024605 (2004).
11. C. H. Dasso *et al.*, Phys. Rev. C **39**, 2073 (1989).
12. L. Corradi *et al.*, J. Phys. G: Nucl. Part. Phys. **36**, 113101 (2009).
13. V. Zagrebaev *et al.*, J. Phys. G: Nucl. Part. Phys. **34**, 1 (2007).
14. M. Evers *et al.*, Phys. Rev. C **81**, 014602 (2010).
15. F. Videbaek *et al.*, Phys. Rev. C **15**, 954 (1977).
16. H. Timmers, Ph.D. thesis, The Australian National University (1996).
17. L. R. Gasques *et al.*, Phys. Rev. C **76**, 024612 (2007).
18. M. Evers *et al.*, Phys. Rev. C **84**, 054614 (2011).
19. M. Evers *et al.*, EPJ Web of Conferences **17**, 08003 (2011).
20. R. M. DeVries *et al.*, Phys. Rev. Lett. **35**, 835 (1975).
21. H. Hasan *et al.*, Nucl. Phys. A **318**, 523 (1979).
22. I. J. Thompson *et al.*, Nucl. Phys. A **505**, 84 (1989).
23. T. Tamura *et al.*, Phys. Rep. **65**, 345 (1980).
24. C. Simenel, Phys. Rev. Lett. **105**, 192701 (2010).
25. A. Winther, Nucl. Phys. A **572**, 191 (1994).
26. A. Winther, Nucl. Phys. A **594**, 203 (1995).
27. S. Szilner *et al.*, Phys. Rev. C **71**, 044610 (2005).